Feedback Control for Perturbations in Blood Flow Total Artificial Heart

Jeevan Karandikar, Li Gong, Shadee Hemaidan, Henry Rose, Emily Schuler

***Abstract*— The Total Artificial Heart (TAH) is a pneumatically powered mechanical circulatory support system designed to replace a patient's heart ventricles and valves. The TAH can be used in severe and cases of end-stage heart failure to bridge the gap between getting a heart transplant [3]. Therefore, this paper explores a feedback control system that models the systemic blood flow in the total artificial heart, building upon previously conducted research published in the American Society for Artificial Internal Organs (ASAIO) Journal. The model found in literature modeled the blood flow in both the pulmonary circuit, taking blood into the lungs, and the systemic system which transports blood to and from the body in the heart [6]. This model, while thorough, made analsysi conplicated due to the sheer number of variables and factors affecting the overall system. Furthermore, the ASAIO model contained only integral feedback control, which kept DC error at 0% [6], but created unwanted oscillations in responses. Therefore, the model we propose in this paper focuses only on the systematic circuit and contains both proportional and derivative control. Our new model helped to increase the phase margin and stability while also allowing for faster responses to sudden changes in the system. Future considerations would be to add proportional and derivative control to the entire model of the total artificial heart.**

I. INTRODUCTION

The heart functions as a pump, circulating blood throughout the body to deliver oxygen and nutrients to organs, tissues, and muscles while removing waste products. Deoxygenated blood flows into the right atrium and through the pulmonary circuit for oxygenation. Oxygenated blood is pumped from the left ventricle into the systemic circuit to sustain bodily functions [6].

The heart itself is made up of four chambers. Deoxygenated blood filled with waste products from the body flows through the superior vena cava into the right atrium, then into the right ventricle, and out to the lungs through the pulmonary artery. The blood goes through a gas exchange in the lungs, picking up oxygen and removing CO_2 waste [5]. The oxygenated blood then reenters the heart through the pulmonary vein into the left atrium, then left ventricle, and finally is delivered to the rest of the body out of the aorta [5].

Heart disease remains one of the leading causes of death globally, with coronary artery disease being a primary contributor [2]. This condition, characterized by the narrowing or blockage of coronary arteries, increases the likelihood of heart attacks and presents a significant public health challenge. In the United States, heart disease accounts for a considerable proportion of mortality among both men and women, emphasizing the urgent need for advanced therapeutic solutions [2].

One such solution to address severe cases, the total artificial heart (TAH) is a pneumatically powered mechanical circulatory support system designed to replace the patient's ventricles and valves [3]. Currently, the TAH is approved as a bridge to heart transplantation and provides critical support for patients with end-stage biventricular heart failure. The TAH provides critical support for patients awaiting donor hearts, thereby enhancing survival rates and quality of life.

The systemic circulation, a cornerstone of the cardiovascular system, underpins the effectiveness of devices like the TAH. This intricate network begins with oxygen-rich blood being pumped from the left ventricle through the aorta to the body and culminates in the return of deoxygenated blood to the heart [4]. This cycle not only delivers essential nutrients to organs and tissues but also facilitates the removal of waste products, maintaining homeostasis.

Central to the systemic circulation are the mechanical properties of resistance and compliance. These attributes govern blood flow dynamics, with the left ventricle's pumping action playing a predominant role in initiating and sustaining systemic blood flow. Modeling the systemic circuit as a simplified electrical circuit offers valuable insights into its functional dynamics. By isolating the contributions of resistance and compliance, researchers can simulate and predict perturbations in flow rates under various conditions, aiding in the design of more effective interventions.

The importance of this research lies in its potential to enhance our understanding of heart and vasculature-related diseases. By unraveling the complexities of systemic blood flow and identifying the factors that disrupt it, we can develop more precise diagnostic tools and treatment strategies. This line of inquiry is particularly relevant for refining artificial heart technologies, ensuring that they replicate physiological blood flow patterns as closely as possible, and ultimately improving patient outcomes.

II. METHODS

A. System Modeling and Analysis Approach

This study focuses on modeling and analyzing the systemic circuit blood flow in a continuous flow total artificial heart (CFTAH) using a simplified control system. The CFTAH replaces the heart's natural ventricles with two continuous flow pumps (CFPs). In this analysis, we concentrate on the left pump, which drives oxygenated blood through the systemic circulation, treating the system as an electrical analog. Vascular resistance (R), compliance (C), and blood flow rate (Q) are represented by electrical resistance, capacitance, and current, respectively, with pressure differences (ΔP) analogous to voltage. This abstraction provides a framework

for understanding flow dynamics under physiological and pathological conditions.

In a blood vessel, vascular resistance measures the opposition to blood flow. Mathematically, it is defined as:

$$R = \frac{8\eta L}{\pi r^4} \tag{1}$$

where R is resistance, η represents blood viscosity, L is the vessel length, and r is the vessel radius [4].

Blood flow (Q) through vessels is driven by pressure gradients:

$$Q = \frac{\Delta P}{R} \tag{2}$$

where ΔP is the pressure difference between two points in the vessel.

Vessel compliance (C) characterizes the vessel's ability to expand and accommodate volume changes:

$$C = \frac{\Delta V}{\Delta P} \tag{3}$$

This relationship can be expressed dynamically as:

$$C\frac{dP}{dt} = \frac{dV}{dt} \tag{4}$$

B. Original System Model

The original model proposed by Khalil et al. [1] divided the circulatory system into left and right sides, with each side containing its respective pump and circulation pathway.

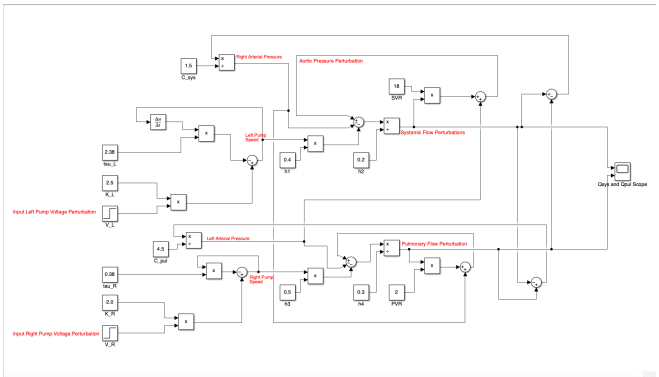

Fig. 1. Full-scale Simulink implementation of the total artificial heart system, detailing the coupling of both circuits of the circulatory system.

The model captures the dynamics of both pulmonary and systemic circuits, including the interactions between right and left pumps, compliance chambers, and vascular resistance elements. The perturbations in blood flow are modeled through transfer functions representing the coupled dynamics of both circuits.

This complete model incorporated both systemic and pulmonary circuits, resulting in a set of coupled differential equations describing the system dynamics. The full-scale model describes the physical phenomena based on the following key assumptions:

- Blood flow can be treated as a continuous fluid with constant viscosity
- Vascular compliance behaves linearly within the operating range
- Pump dynamics can be approximated by first-order transfer functions
- Flow perturbations in both circuits are coupled through the pump interactions

The transfer function matrix for the complete system relates input voltages to output flow rates:

$$\begin{bmatrix} Q_{sys} \\ Q_{pul} \end{bmatrix} = \begin{bmatrix} a_{11} & a_{12} \\ a_{21} & a_{22} \end{bmatrix} \begin{bmatrix} V_L \\ V_R \end{bmatrix} \tag{5}$$

C. Simplified Model Development

Rather than analyzing the complete coupled system, we focused our investigation on the left pump's contribution to systemic circulation. This approach is not so much a simplification as it is an isolation of specific dynamics of interest.

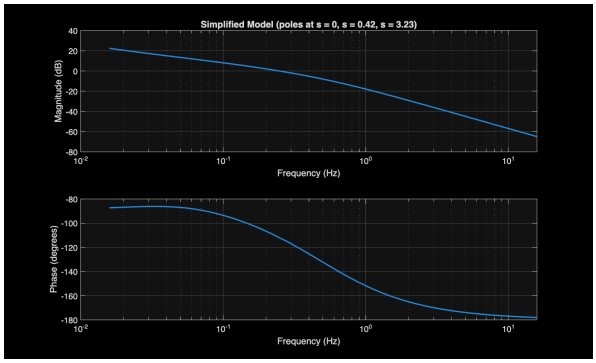

Fig. 2. Simplified analysis model focusing on the left pump dynamics and systemic circuit.

The above figure describes the relationship between left pump voltage (V_L) and systemic flow rate (Q_{sys}), thereby isolating the a_{11} H(s) bio-system transfer function. While this approach focuses on a subset of the full dynamics, it maintains the essential characteristics of the left pump's influence on systemic circulation.

By focusing on the a_{11} transfer function, we analyzed how left pump voltage perturbations affect systemic flow rate:

$$Q_{sys} = a_{11}V_L \tag{6}$$

This focused analysis allowed us to:

- Examine the direct relationship between pump input and systemic flow
- Design and evaluate control strategies specifically for left pump operation
- Analyze stability characteristics without the complexity of coupled dynamics
- Maintain physiological relevance while reducing analytical complexity

The linearized equations (refer to Appendix), determined through step responses of a mock circulatory system [1], establish the baseline behavior of the system. These equations incorporate:

- Steady-state pulmonary artery pressure

- Aortic pressure
- Systemic vascular resistance
- Pulmonary vascular resistance

D. Control System Design

The control strategy evolved through several stages:

1) Initial integral control from measurement error function $g(s) = 1.7/s$
2) Addition of proportional-derivative (PD) control to improve stability
3) Investigation of various pole placements and their effects
4) Implementation of full PID control with strategic pole cancellation

The final controller parameters were selected based on stability requirements and performance goals:

- $K_d = 1$ for derivative control
- $K_p = 0.42$ for proportional gain
- $K_i = 1.7$ maintained from original integral control

See the appendix for the full derivation.

E. Operational Constraints

The system operates under specific constraints to ensure physiological relevance:

- Baseline systemic vascular resistance: 18 Wood units
- Target systemic flow rate (Q_{sys}): 4 L/min
- Non-pulsatile flow assumption
- Linear operation around steady-state conditions

III. RESULTS

A. Transfer Function Analysis

The transfer function analysis revealed key characteristics of the system's behavior:

TABLE I
PHASE MARGIN ANALYSIS RESULTS FOR DIFFERENT CONTROL CONFIGURATIONS

Model	Phase Margin (°)	ω_{cp} (Hz)
Simplified Model	68.169	0.24714
PID Control (2 poles at $s = 0$)	86.867	0.90126
PD Control (poles at $s = 0.42$, $s = 0$)	91.111	0.89873
PD Control (poles at $s = 3.23$, $s = 0$)	120.94	0.74096

B. Control Strategy Analysis

Instead of conducting a traditional sensitivity analysis with varying controller parameters, we focused on comparing fundamentally different control approaches. Using the derived ratios of K_p, K_d, and K_i from our mathematical analysis (see Appendix), we investigated three distinct control strategies:

1. PD control targeting the removal of the $s = -3.23$ pole 2. Alternative PD control targeting the removal of the $s = -0.42$ pole 3. PID control attempting to remove both poles

This strategic comparison allowed us to evaluate the system's behavior under different pole placement scenarios rather than examining sensitivity to parameter variations. Each control strategy maintained the mathematically derived ratios between parameters while pursuing different control objectives.

The Simulink implementations and subsequent Bode analysis demonstrate that the choice of which poles to cancel had a more significant impact on system performance than variations in individual control parameters. Notably:

- PD control removing $s = -3.23$ achieved optimal stability
- Attempting to remove $s = -0.42$ led to increased oscillations
- Full PID control, while theoretically capable of removing both poles, introduced destabilizing double integration

C. Simulink Model Analysis

The control system was implemented in Simulink to validate the theoretical analysis and examine the system behavior under various pole placement strategies. For all simulations, we used a pulse generator with amplitude of 0.5 V and frequency of 400 Hz as the input voltage signal, following the parameters established in Khalil et al. [1]. We developed four different configurations to analyze the effects of pole cancellation and control strategy on system performance.

1) Original Simplified Model: The simplified model derived from Khalil et al. [1] was implemented first, representing the baseline system with poles at $s = 0$, $s = -0.42$, and $s = -3.23$:

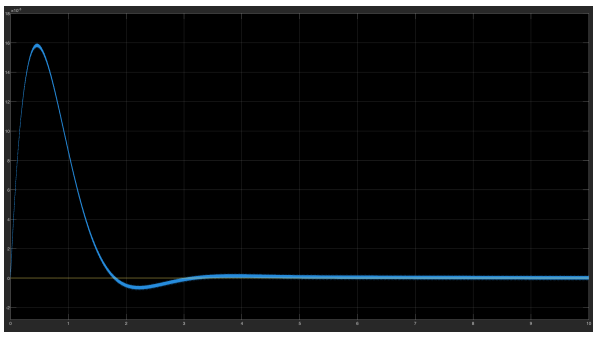

Fig. 3. Step response of the simplified model showing initial overshoot followed by stable convergence. The system exhibits characteristic second-order behavior with a peak overshoot of approximately 16×10^{-3} at $t = 0.5s$ before settling to steady state.

2) PD Control Strategy with s=-3.23 Removal: The first control modification implemented PD control to cancel the pole at $s = -3.23$, leaving poles at $s = 0$ and $s = -0.42$:

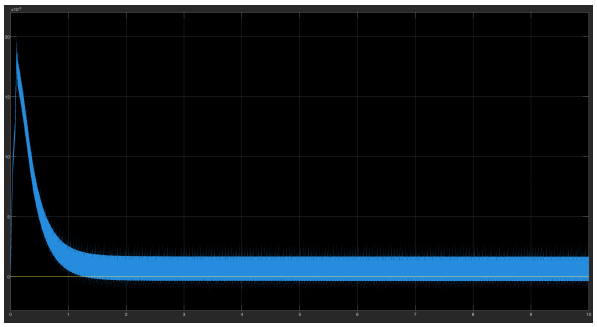

Fig. 4. System response with PD control ($K_p = 0.42$) showing improved damping characteristics. The response exhibits reduced overshoot compared to the simplified model while maintaining stability.

3) Alternative PD Control with s=-0.42 Removal: An alternative PD control strategy was implemented to cancel the pole at $s = -0.42$, retaining poles at $s = 0$ and $s = -3.23$:

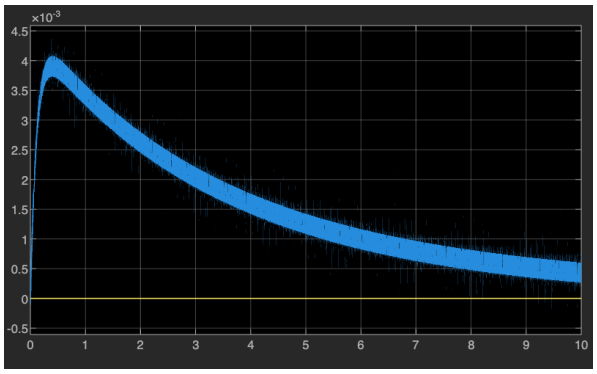

Fig. 5. System response with alternative PD control showing faster initial response but with increased oscillatory behavior. High-frequency noise is more pronounced due to the remaining high-frequency pole.

4) PID Control with Double Integration: Finally, a PID controller was implemented that removed both poles at $s = -0.42$ and $s = -3.23$ but introduced a second pole at $s = 0$:

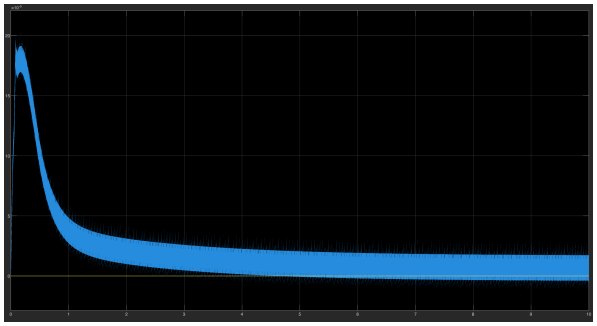

Fig. 6. System response with PID control showing significant high-frequency oscillations and decreased stability as a byproduct of the double integration presence.

The Simulink implementations utilized the controller parameters derived in Appendix A, with the PD and PID controllers designed to achieve specific pole cancellation. The simulation results demonstrate that:

- The PD control strategy removing the $s = -3.23$ pole provides the best balance of stability and performance
- Attempting to cancel the $s = -0.42$ pole results in increased high-frequency oscillations
- The double integrator configuration (PID with two poles at $s = 0$) exhibits poor stability characteristics
- All configurations maintain zero steady-state error due to the presence of at least one integrator

These time-domain simulation results complement the frequency-domain analysis presented in the following Bode plot analysis section, confirming the theoretical predictions about system stability and performance.

D. Frequency Response Analysis

The Bode plot analysis demonstrated distinct characteristics for each control strategy:

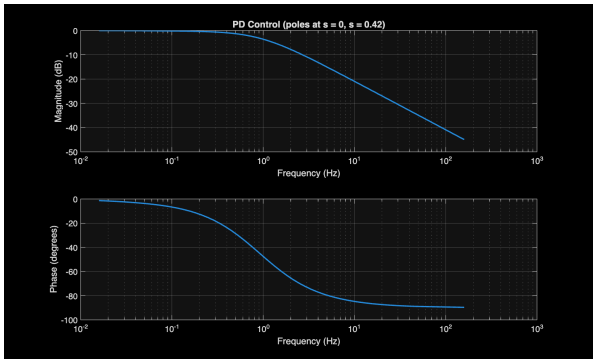

Fig. 7. Bode plot for PD control with poles at $s = 0$ and $s = 0.42$, showing improved phase margin.

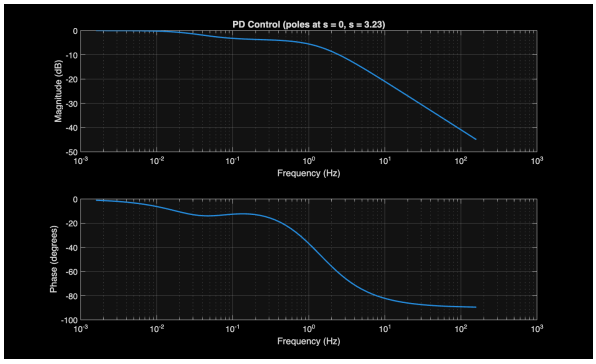

Fig. 8. Bode plot for PD control with poles at $s = 0$ and $s = 3.23$, demonstrating enhanced stability.

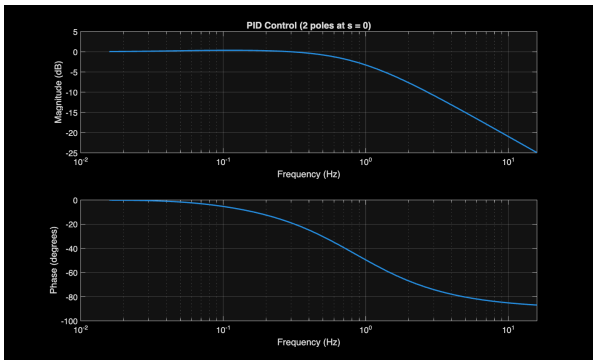

Fig. 9. Bode plot showing degraded performance with double integrator effect.

Key findings from the frequency response analysis:

- All configurations achieved zero DC error due to integral control
- PD control removing the $s = 3.23$ pole showed optimal phase margin (120.94°)
- Double integration (two poles at $s = 0$) demonstrated unstable behavior
- Crossover frequencies remained physiologically appropriate (< 1 Hz)

IV. DISCUSSION

A. Simulation Limitations and Error Analysis

The primary sources of potential error in our simulation stem from various simplifying assumptions and approximations. First, the linearization of the system around steady-state conditions is an approximation, and it may fail to capture the non-linear dynamics that become significant during large perturbations or extreme physiological changes. Conditions such as severe blood loss can push the system beyond the range where linearization is valid.

Additionally, our model does not account for complex vascular dynamics. The cardiovascular system operated upon intricate feedback mechanisms between the systemic and pulmonary circuits. For example, cardiac output is dependent on venous return, and venous return is dependent on peripheral resistance and blood volume. A decrease in peripheral resistance during exercise can increase venous return to the heart, increasing stroke volume and cardiac output. Our model treats these as mostly constant. Consequently, the model's accuracy is limited under varying physiological conditions.

Moreover, our model assumes that blood flow is continuous. In reality, blood flow is pulsatile due to contractions of the heart. Non-pulsatile flow generated by continuous-flow devices has been associated with increased peripheral vascular resistance, endothelial dysfunction, and arterial stiffening, potentially leading to complications like gastrointestinal bleeding, aortic regurgitation, and hypertension [7].

B. Physiological Relevance

The simulation results match expected physiological behavior. The model successfully maintains constant flow rates under varying conditions, reflecting the cardiovascular system's ability to regulate blood flow despite changes in resistance or pressure gradients. This is critical for ensuring consistent tissue perfusion during mild physiological stress.

The model also demonstrates appropriate response times to perturbations, replicating the rapid adjustments the cardiovascular system makes during changes, such as shifts in posture. Stability within physiological pressure ranges further supports the relevance of the simulation, as it captures the necessary balance to sustain effective systemic and pulmonary circulation without causing excessive strain.

Finally, the simulation produces realistic flow rate perturbations in response to changes in resistance.

These features highlight the physiological relevance of the model and its potential as a tool for studying cardiovascular dynamics and evaluating the Total Artificial Heart (TAH).

C. Clinical Applications

The model effectively simulates systemic hypertension by modifying vascular resistance parameters. This pathological condition provides insights into controller performance under stressed conditions and suggests potential therapeutic strategies.

D. Simulation Benefits and Limitations

Advantages of simulation approach:

- Safe exploration of extreme conditions
- Rapid iteration of control strategies
- Cost-effective testing of multiple scenarios
- Detailed analysis of system dynamics

Limitations:

- Simplified representation of complex biological systems
- Inability to capture all physiological variables
- Limited validation against in vivo conditions
- Assumptions about linear behavior

V. CONCLUSION

This study demonstrates the effectiveness of simplified control strategies for continuous flow total artificial hearts. The PD control approach, particularly with strategic pole placement, achieves superior stability while maintaining physiological flow rates. The insights gained from this analysis contribute to the ongoing development of more reliable artificial heart control systems, potentially improving outcomes for patients with end-stage heart failure.

APPENDIX

A. Linearized ODEs

Linearized ODEs around small perturbations, δ [1]:

$$\delta Q_{sys} - \delta Q_{pul} = C_{sys}\delta \mathrm{RAP}, \quad \text{(A1)}$$

$$\delta Q_{pul} - \delta Q_{sys} = C_{pul}\delta \mathrm{LAP}, \quad \text{(A2)}$$

$$\delta \mathrm{AoP} - \delta RAP = \mathrm{SVR}\delta Q_{sys}, \quad \text{(A3)}$$

$$\delta \mathrm{PAP} - \delta LAP = \mathrm{PVR}\delta Q_{pul}, \quad \text{(A4)}$$

$$\delta AoP - \delta LAP = h_1\delta\omega_L + h_2\delta Q_{sys}, \quad \text{(A5)}$$

$$\delta PAP - \delta RAP = h_3\delta\omega_R + h_4\delta Q_{pul}, \quad \text{(A6)}$$

$$\tau_L\delta\dot{\omega}_L + \delta\omega_L = K_L\delta V_L, \quad \text{(A7)}$$

$$\tau_R\delta\dot{\omega}_R + \delta\omega_R = K_R\delta V_R, \quad \text{(A8)}$$

Variables:
h1,2,3,4: experimentally determined constants
AoP:aortic pressure
PaP:pulmonary artery pressure
Qsys:systemic blood flow rate (L/min)
Qpul:pulmonary blood flow rate (L/min)
SVR: systemic vascular resistance
PVR=pulmonary vascular resistance
ω_L, ω_R:left and right pump speeds, respectively
Csys: systemic capacitance
Cpul: pulmonary capacitance
$V_L V_R$: left and right pump input voltages, respectively
K_L, K_R: experimentally determined constants

Fig. 10. Linearized ODEs around small perturbations to model TAH.

PID control Transfer Function:

$$F(s) = K_d s + K_p + \frac{K_i}{s} = \frac{K_d s^2 + K_p s + K_i}{s} \tag{7}$$

Zeros:

$$s = -\frac{K_p}{2K_d} \pm \frac{\sqrt{K_p^2 - 4K_d K_i}}{2K_d} \tag{8}$$

Poles

$$s = 0 \tag{9}$$

PD control Transfer Function:

$$F(s) = K_d s + K_p = K_d \left(s + \frac{K_p}{K_d} \right) \tag{10}$$

Zeros:

$$s = -\frac{K_p}{K_d} \tag{11}$$

Poles: None.

Open-Loop Transfer Function:

The open-loop transfer function of the total artificial heart is modeled by H(s):

$$H(s) = 0.76 \cdot \frac{\frac{s}{0.31} + 1}{(\frac{s}{0.42} + 1)(\frac{s}{3.23} + 1)} \tag{12}$$

Simplified:

$$H(s) = \frac{0.76}{0.31} \cdot (0.42) \cdot (3.23) \cdot \frac{s + 0.31}{(s + 0.42)(s + 3.23)} \tag{13}$$

Zeros:

$$s = -0.31 \tag{14}$$

Poles:

$$s = -0.42, -3.23 \tag{15}$$

Adding PID control can cancel both poles at s = -0.42 and s = -3.23, but it will add an additional pole at s = 0. Adding PD control only cancels one pole – based on our Bode plots, we decided to cancel the pole at s = -0.42:

$$\frac{K_p}{K_d} = 0.42 \tag{16}$$

$$K_d = \frac{K_p}{0.42} \tag{17}$$

The TAH comes with integral control $G(s)$ where $K_i = 1.7$:

$$G(s) = \frac{1.7}{s} \tag{18}$$

Assume $K_d = 1$, K_p is calculated as:

$$1 = \frac{K_p}{0.42} \tag{19}$$

$$K_p = 0.42 \tag{20}$$

ACKNOWLEDGMENT

We would like to thank our professor, Dr. Gert Cauwenberghs and our BENG 122a TAs, Benjamin Balster and Melody Hseih, for their support and guidance throughout the quarter and with this project.

REFERENCES

[1] H. A. Khalil, D. T. Kerr, M. A. Franchek, R. W. Metcalfe, R. J. Benkowski, W. E. Cohn, E. Tuzun, B. Radovancevic, O. H. Frazier, and K. A. Kadipasaoglu, "Continuous Flow Total Artificial Heart: Modeling and Feedback Control in a Mock Circulatory System," *ASAIO Journal*, vol. 54, no. 3, pp. 249–255, May 2008. DOI: 10.1097/MAT.0b013e3181739b70

[2] B. R. Raiff, C. A. Burrows, J. A. Nastasi, C. R. Upton, and M. J. Dwyer, "A behavioral approach to the treatment of chronic illnesses," *Functional Analysis in Clinical Treatment*, pp. 501–532, 2020. [Online]. Available: https://doi.org/10.1016/b978-0-12-805469-7.00021-8

[3] J. A. Cook, K. B. Shah, M. A. Quader, R. H. Cooke, V. Kasirajan, K. K. Rao, M. C. Smallfield, I. Tchoukina, and D. G. Tang, "The total artificial heart," *Journal of Thoracic Disease*, vol. 7, no. 12, pp. 2172–2180, Mar. 2017. DOI: https://doi.org/10.3978/j.issn.2072-1439.2015.10.70

[4] L. M. Biga, S. Bronson, S. Dawson, A. Harwell, R. Hopkins, J. Kaufmann, M. LeMaster, P. Matern, K. Morrison-Graham, K. Oja, D. Quick, J. Runyeon, O. Oeru, and OpenStax, "20.2 Blood flow, blood pressure, and resistance," *Anatomy Physiology*, Open Oregon State, Sept. 26, 2019. [Online]. Available: https://open.oregonstate.education/aandp/chapter/20-2-blood-flow-blood-pressure-and-resistance/

[5] G. Cauwenberghs, "BENG 122A Lecture Notes, Lecture 2," 2024. [Online]. Available: Beng122a-lecture2.pdf

[6] Cleveland Clinic, "Circulatory System," accessed Dec. 12, 2024. [Online]. Available: https://my.clevelandclinic.org/health/body/circulatory-and-cardiovascular-system

[7] S. N. Purohit, W. K. Cornwell, J. D. Pal, J. Lindenfeld, and A. V. Ambardekar, "Living without a pulse: The vascular implications of continuous-flow left ventricular assist devices," *Circ. Heart Fail.*, vol. 11, no. 6, p. e004670, Jun. 2018. [Online]. Available: https://pmc.ncbi.nlm.nih.gov/articles/PMC6007027/